To cite this article: HUANG L, CHEN Y H, ZENG K, et al. Influence of ship wake on hydrodynamic performance of cycloidal propeller [J/OL]. Chinese Journal of Ship Research, 2022, 17(1). http://www.ship-research.com/en/article/doi/10.19693/j.issn.1673-3185.02151.

DOI: 10.19693/j.issn.1673-3185. 02151

Influence of ship wake on hydrodynamic performance of cycloidal propeller

HUANG Lu, CHEN Yihong, ZENG Ke, LIU Zhuqing*

China Ship Scientific Research Center, Wuxi 214082, Jiangsu, China

Abstract: [**Objective**] The cycloidal propeller is a special propeller which generates thrust by means of profiled blades that protrude from the hull of the vessel and rotate around a vertical axis, allowing precise and step-less thrust generation. It is necessary to study the hydrodynamic performance of cycloidal propeller in open-water and hull wake conditions. [**Methods**] By analyzing the operating principle of the cycloidal propeller, a formulas for the multiple motion laws of the blades is derived. The open-water performance of cycloidal propeller is then calculated using the RANS equation and k-ε turbulence model based on a sliding grid. Comparison with the experimental data verifies the accuracy of the hydrodynamic performance prediction method of cycloidal propeller. The propellor's unsteady hydrodynamic performan in a ship's hull wake is also investigated. [**Results**] The results show that the force on the cycloidal propeller and singlar blade has blade frequency characteristics; the fluctuation amplitude of the thrust and torque increase with the increase of the advanced coefficient; the lateral force is significantly affected by the hull wake, while the thrust and torque are slightly affected. [**Conclusions**] The results of this study have important reference value for research on blade strength evaluation and blade design optimization.

Key words: cycloidal propeller; multiple motion of blades; hull wake; hydrodynamic performance

CLC number: U664.35

0 Introduction

The cycloidal propeller serves as a special marine propeller that can generate thrust and steering force ranging from 0 to the maximum in any direction. The propeller generates thrust through the blades that project from the bottom of the ship and performs oscillating motion around the vertical axis, which is installed on the rotating box flush with the bottom of the ship[1]. By the linkage mechanism, each blade makes local oscillating motion around its own axis while oscillating around the common vertical axis shared by all blades. As a result, the thrust generated by the dual oscillating motion will be superimposed on the rotating box. In the case of a conventional propeller, the direction of the thrust and the axis of rotation are identical, while in the case of a cycloidal propeller, they are perpendicular to each other. Therefore, the cycloidal propeller generated thrust comes in no preferential direction, and its size and direction are allowed to be step-less and adjustable. As only the blades extend beyond the hull, the installation of the whole system is spared from the impact of the resistance of appendages, such as the rudder and propeller axis[2].

In the early days, many scholars studied the prediction of hydrodynamic performance of cycloidal propellers by various theoretical methods, which, according to the theoretical basis of mathematical models, are generally classified into four categories: 1) the calculation method for hydrodynamic performance of cycloidal propeller based on lift line

Received: 2020－10－20 **Accepted**: 2021－02－28

Supported by: Project of the National Ministries and Commissions of China

Authors: HUANG Lu, female, born in 1990, master's degree, engineer
CHEN Yihong, male, born in 1980, master's degree, professor
ZENG Ke, male, born in 1989, Ph.D., engineer
LIU Zhuqing, female, born in 1982, master's degree, senior engineer

***Corresponding author**: HUANG Lu

theory; 2) the calculation method for hydrodynamic performance of cycloidal propeller based on the theorem of momentum; 3) the calculation method for hydrodynamic performance of cycloidal propeller based on vortex theory; 4) the numerical calculation method for hydrodynamic performance of cycloidal propeller based on viscous CFD[3]. Considering the complex multiple motion of cycloidal propeller blades, the current research in China and other countries focuses mainly on the performance analysis of the time-averaged force on blades[4]. Meanwhile, as the rotation axis of cycloidal propeller is placed at the rear of the ship along the line perpendicular to the hull, the acceleration of the stern fluid can lead to the change in the stern pressure distribution during operation and thus affect the distribution of the hull resistance, the thickness of the stern boundary layer, and the speed distribution within the boundary layer. The change in the boundary layer can influence the inflow conditions of a propeller, which may bring about relevant problems such as cavitation[5] and noise[6]. Therefore, it is necessary to study the unsteady hydrodynamic performance of cycloidal propeller and the influence of hull wake on their hydrodynamic performance.

By analyzing the operating principle of cycloidal propeller, this paper intends to derive the formulas of the multi-motion law of blades and then calculate the open-water performance of cycloidal propeller on the basis of the RANS equation and k-ε turbulence model. Moreover, it performs a comparison with the test values to verify the accuracy of the method for the prediction of hydrodynamic performance of cycloidal propeller. In the meanwhile, considering the influence of hull wake, it also studies the influence of hull wake on the unsteady hydrodynamic performance of cycloidal propeller through the grid refinement strategy for the key area of the stern.

1 Operating principle and hydrodynamic expression for cycloidal propeller

1.1 Operating principle of cycloidal propeller

The blades of a cycloidal propeller make circular motion around the central axis while making oscillating motion around their own axis. As shown in Fig. 1, a blade is controlled by the internal linkage mechanism during the motion so that its chord remains always perpendicular to the connecting line from the axis center of the blade to a certain point N, with the point N known as the eccentric point. The distance from the control point N to the center O of a circle is the eccentric distance ON, and the ratio of the eccentric distance ON to the revolution radius R of the blade is the eccentricity e ($e = ON/R$). Accordingly, it is deduced that the motion law of the oscillatory angle of the blade can be written as

$$\omega_c = \frac{e \cdot \cos\theta + e^2}{1 + 2e\cos\theta + e^2} \cdot \omega \tag{1}$$

where ω_c is the angular velocity of the blade oscillatory angle around its axis; ω is the rotational angular velocity of the blade rotating around the central axis; θ is the rotation angle of the blade around the central axis.

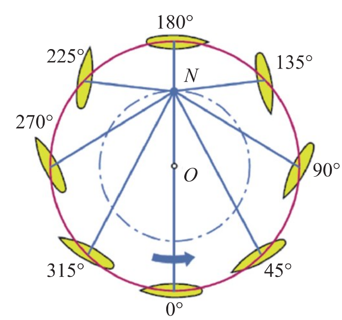

(a) Relationship between blade angle change and the control point

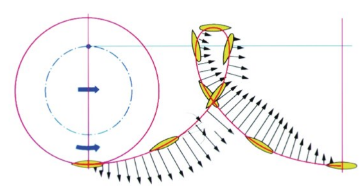
(b) Change in lift force when the blade finishes a cycle of rotation

Fig. 1 Lift force distribution on the blade

1.2 Hydrodynamic expressions for cycloidal propeller

When a blade rotates, its chord always remains at a positive angle of attack with the direction of inflow except at the positions of 0° and 180° to generate lift force. The component of the lift force in the forward direction is the thrust, and that perpendicular to the forward direction is the side thrust, with the resultant moment of the lift force and resistance of the blade to the center of the turntable as the torque. The main thrust T, side thrust S, and torque Q of a cycloidal propeller represent the superposition of the average main thrust, average side thrust, and average torque of each blade rotating for one cycle[7], respectively. They can be expressed by dimensionless coefficients to characterize the hydrodynamic characteristics of the cycloidal propeller. In the dimensionless expressions, unlike the constant factors of the propeller, cycloidal propeller integrates the blade length L into the corresponding thrust and torque coefficients. Thus, the main thrust coefficient K_T, side thrust coefficient K_S, torque coefficient K_Q, efficiency η, and advance coefficient J can be expressed as

$$K_T = \frac{T}{\rho n^2 D^3 L} \tag{2}$$

$$K_S = \frac{S}{\rho n^2 D^3 L} \tag{3}$$

$$K_Q = \frac{Q}{\rho n^2 D^4 L} \tag{4}$$

$$\eta = \frac{J}{2\pi} \cdot \frac{K_\mathrm{T}}{K_\mathrm{Q}} \tag{5}$$

$$J = \frac{V}{nD} \tag{6}$$

where ρ is the fluid density; n is the rotational speed of the cycloidal propeller; D is the swing diameter of the cycloidal propeller; V is the velocity of inflow.

2 Method for hydrodynamic numerical simulation of cycloidal propeller

2.1 Governing equation

This paper simulates the viscous flow field around a cycloidal propeller and seeks the solution by the unsteady RANS solver STAR-CCM+12.0. To solve the RANS equation, each dependent variable ϕ (including parameters such as velocity and pressure) is decomposed into the mean $\bar{\phi}$ and pulsation value ϕ' in the instantaneous N-S equation.

The transport equation of mass and momentum of the average physical quantity can be expressed as

$$\frac{\partial \rho}{\partial t} + \nabla \cdot (\rho \bar{V}) = 0 \tag{7}$$

$$\frac{\partial \left(\rho \bar{V}\right)}{\partial t} + \nabla \cdot \left[\rho \bar{V}\left(\bar{V}\right)\right] = -\nabla \cdot \bar{P}\boldsymbol{I} + \nabla \cdot (\boldsymbol{T} + \boldsymbol{T}_t) + f_\mathrm{b} \tag{8}$$

where $\bar{V}$ and $\bar{P}$ is the average velocity and average pressure, respectively; $\boldsymbol{I}$ is the unit tensor; $\boldsymbol{T}$ is the tensor of viscous stress; $\boldsymbol{T}_t$ is the Reynolds stress tensor; f_b is the resultant of volume force including gravity and centrifugal force; and t is the time.

As the term of Reynolds stress tensor in the momentum equation discloses the governing equation, it is required to introduce the turbulence model for solutions. This paper selects the k-ε turbulence model that is well-developed in theory and widely applied in engineering to close the RANS equation[8].

On the basis of the SIMPLE algorithm, the separated iterative method adopts the second-order upwind scheme to discretize the convective term in the RANS equation and then uses the second-order Euler implicit scheme for time integration. The near-wall boundary layer flow is solved by the wall function, and the time step is set according to the 1° revolution for each time step, with 15 iterative calculations made in each time step.

2.2 Grid model

As the blades of cycloidal propeller report dual rotation—revolution and autorotation, we adopt the double sliding grid method to perform the functions of cycloidal propeller, as shown in Fig. 2. First, we set a small cylindrical domain with a diameter of 0.25D and a height of 0.6D near each blade with the rotation axis of the blade as the center, so as to achieve independent oscillation of the small cylinder and the blade together. Second, we set a large circular rotation domain with a diameter and a height of 0.8D and the center of the whole cycloidal propeller as the center of the circle. We achieve the revolution of the blades with the small cylindrical domain wrapped around the blades rotating around the central axis of the large cylindrical domain.

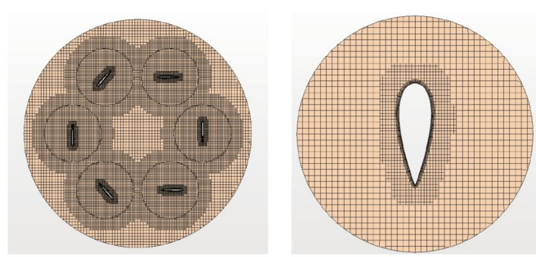

(a) Grids of the propeller area (b) Grids of the area near the blade

Fig. 2 Sliding grids of cycloidal propeller

3 Hydrodynamic numerical prediction of cycloidal propeller

3.1 Calculation objects and grids

As the most comprehensive test report in research on the performance of cycloidal propeller, the No. 2 938 report published by Ficken et al.[9] of the Naval Ship Research and Development Center, the U.S. Department of the Navy, in 1969 elaborated the test results of the eccentricity of cycloidal propeller, i. e., e = 0.4−0.9. This paper refers to the geometric blades presented in the test report No. 2 938, with the calculated dimensions of the geometric model shown in Table 1 (in the table, C represents the chord length) and the geometric modeling for the calculation model shown in Fig.3.

Table 1 Geometric dimensions of calculation model of cycloidal propeller

Parameter	Value
Propeller diameter D/mm	228.6
Maximum chord length of blades/mm	43.28
Average chord length of blades/mm	40.26
Blade length L/mm	114.3
Blade area S/mm^2	4 601.7
Number of blades	6
L/D	0.5
C/D	0.176

Fig. 3 Geometric model of cycloidal propeller

The rectangular calculation domain reports a distance of 4D from its inlet to the front of the cycloidal propeller, 12D from the outlet to the cycloidal propeller, 4D from its side to the cycloidal propeller, and 4D from its far field of the bottom to the cycloidal propeller. To verify the influence of grid quantities on the calculation and ensure consistent grid topology, we studied Scheme 1 (2.29 million grids) and Scheme 2 (5.08 million grids). To be specific, the benchmark grid scale BS of Scheme 1 is 0.08D, and that of Scheme 2 is 0.06D; the grid scale of blade surface is 6.25%BS, and the maximum scale of the small cylindrical domain wrapped around the blades is 12.5%BS, while the scale of the large cylinder wrapped around the cycloidal propeller is 25%BS. The boundary layer generates six layers of grids, an increase of 120%, with the height of the first-layer grids of the boundary layer determined between 30 and 100 according to the Y^+ value. It is found through calculations that the two sets of grids report a calculation error of 3.71% and 3.57% respectively. Given the efficiency and accuracy of the calculation overall, Scheme 1 is preferred for the meshing.

The inlet boundary was set as the velocity inlet condition, and the top and side of the cuboid of the calculation domain were set as the wall condition, with the outlet boundary defined as the pressure outlet condition; the outer wall of the large cylindrical domain and the intersecting surface between the large and the small cylindrical domains were set as the interfaces, and the blades were set as the non-sliding surface condition.

3.2 Comparison and verification of hydrodynamic coefficients with tests

Fig.4 shows the variation curves of the thrust coefficient and torque coefficient of the cycloidal propeller with the advance coefficient when eccentricity e = 0.5, 0.7, and 0.9. The figure shows that the results of numerical simulation are generally consistent with the test results, with the error of the coefficient of main thrust being about 5% and that of torque coefficient being about 7%. At a certain eccentricity, the thrust coefficient and torque coefficient decrease with the increase in the advance coefficient; at the same advance coefficient, the thrust coefficient and torque coefficient increase with the increase in the eccentricity, and so does the range of the advance coefficient of positive thrust generated by the propeller.

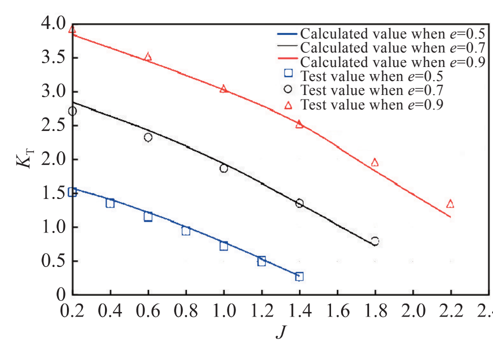

(a) Thrust coefficient

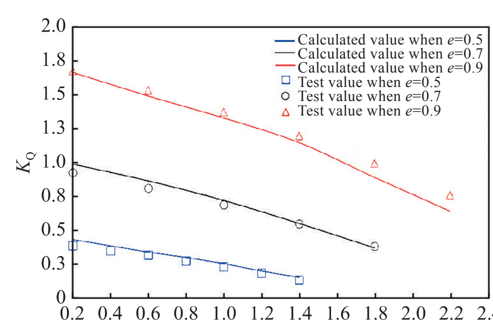

(b) Torque coefficient

Fig.4 Open-water performance of cycloidal propeller

3.3 Variation analysis of single-blade instantaneous load

Fig. 5 shows the variation curve of the main thrust in the rotation of the blades (e = 0.7) for one cycle at different advance coefficients. It can be seen that the fluctuation amplitude of the single-blade load increases with the decrease in the advance coefficient, with the instantaneous load peak recorded at a blade rotation angle of about 300°, and at this time the blades report the largest effective angle of attack. At a blade rotation angle of 0° and 180°, the main thrust is 0, and the blades report a negative oscillatory angle and an effective angle of attack of 0. Fig.6 shows the pressure variation of Blade 1 for one cycle. It is indicated that when the blade rotation angle is 300°, the maximum pressure difference between the pressure surface and the suction surface occurs, which leads to a peak of the instantaneous blade load. At a blade rotation angle of 0° and 180°, however, the minimum pressure difference between the pressure surface and the suction surface appears, and at this time, the main thrust of the blade is 0.

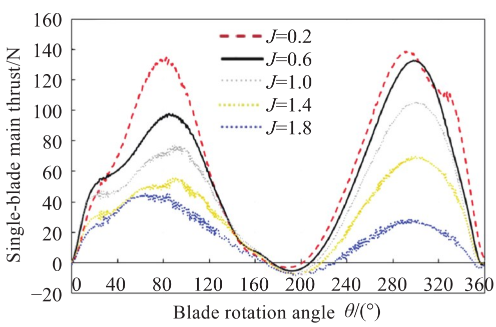

Fig. 5 Variation of instantaneous load of Blade 1 at different advance coefficients (e = 0.7)

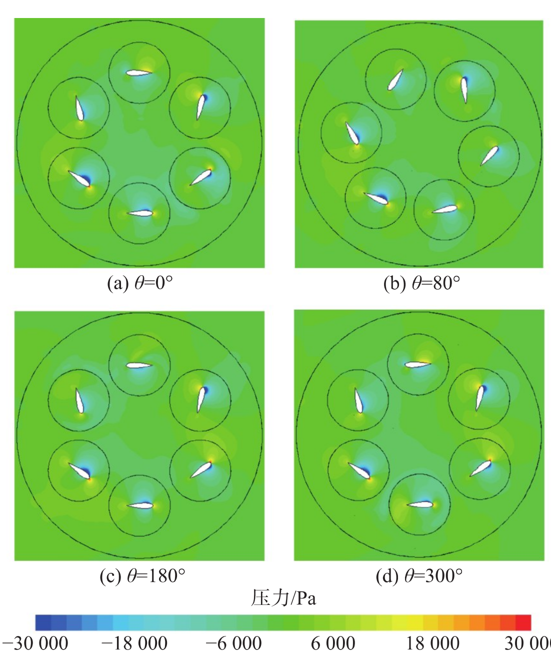

Fig. 6 Variation of pressure distribution of Blade 1

Fig. 7 presents the variation curve of the main thrust of each blade rotating for one cycle. It indicates that each blade reports generally the same load variations. Due to the difference in positional angles between the blades, a phase difference also exists in the variations of the blade load [10]. The peak value of the main thrust of a blade in the first half cycle is lower than that in the second half cycle, because the inflow is accelerated under the induction effect of the blade in the first half cycle, and thus a higher thrust is generated after two rounds of acceleration.

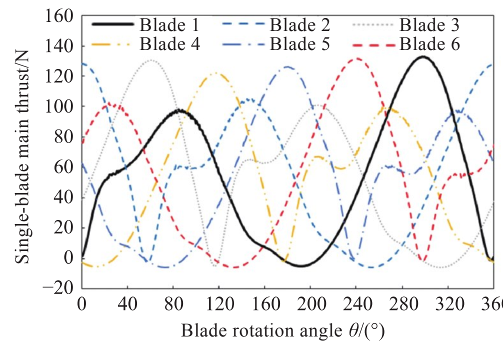

Fig.7 Variation of instantaneous load of a single blade

3.4 Variation analysis of instantaneous load of cycloidal propeller

The instantaneous loads of a cycloidal propeller fluctuate near the time average in practical operation. The main reason is that the changes in the oscillatory angle will lead to the variations of the angle of attack during one cycle of rotation of a single blade, which is accompanied by the force changes, with the superposition of the force on each blade reflected in the instantaneous load fluctuation of the cycloidal propeller. Fig.8 shows the curve variation of the main thrust and torque of the propeller in one rotation cycle when e = 0.7. It can be seen that the main thrust and torque fluctuate periodically with the blade rotation angle, in a period 1/6 of the turning period of the propeller. With the decline in the advance coefficient, the main thrust and torque report an increase in fluctuation amplitude.

4 Hydrodynamic performance of ship-rear cycloidal propeller

4.1 Prediction method for hydrodynamic loads of ship-rear cycloidal propeller

A prediction method for hydrodynamic loads of a ship-rear cycloidal propeller was developed to study the influence of the hull wake on the hydrodynamic performance of the cycloidal propeller. Two cycloidal propellers are symmetrically placed at the stern of the surface ship, with a length of 6.08 m and a draft of 0.28 m, which adopt the research object in Section 3.1.

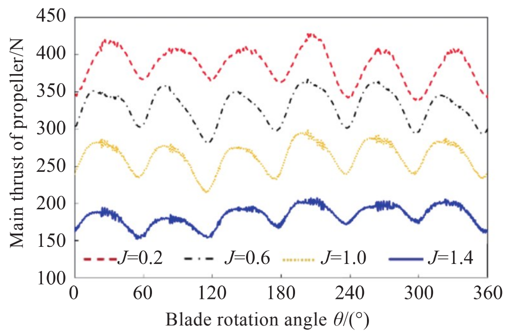

(a) Main thrust of propeller/N

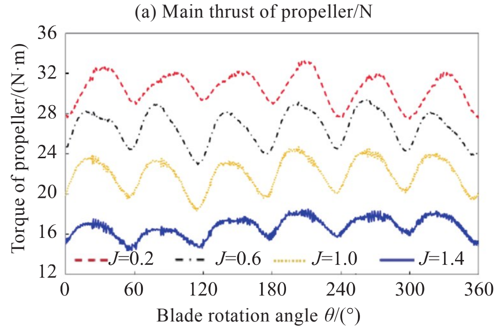

(b) Torque of propeller

Fig. 8 Variation of Instantaneous load of cycloidal propeller (e = 0.7)

The rectangular calculation domain reports a distance of $1.5L_{pp}$ (L_{pp} represents the length between perpendiculars of the hull) from its inlet to the front of the bow, $2.5L_{pp}$ from its outlet to the stern, $1.8L_{pp}$ from its side to the midship, and $1.5L_{pp}$ from its far field of the bottom to the midship. For grid convergence analysis, we calculated the grid quantities of 3.76 million, 6.86 million, and 15.4 million, with the benchmark grid scale of the three sets of grids of $0.438D$, $0.35D$, and $0.263D$, respectively; the maximum grid scale of the hull surface is 25%BS, the grid scale of the blade surface 1.562%BS, the maximum scale of small cylindrical domain wrapped around the blades 3.125%BS, and the scale of the large cylindrical domain wrapped around the cycloidal propeller 6.25%BS. The boundary layer generates six layers of grids, an increase of 120%, with the height of the first-layer grids of the boundary layer determined between 30 and 100 according to the Y^+ value. The calculations indicate that when the quantity of grids is 6.86 million, the numerical prediction can achieve high accuracy and calculation efficiency. Fig. 9 displays the calculation grids of the hull and cycloidal propeller.

4.2 Analysis of hydrodynamic performance of ship-rear cycloidal propeller

Considering the influence of the hull wake, we simulated the ship-rear hydrodynamics of the cycloidal propeller and calculated and compared the

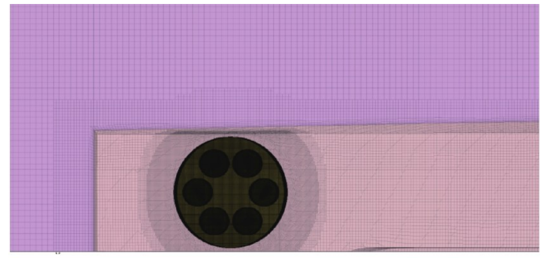

(a) Top view

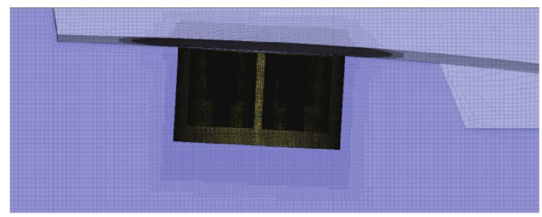

(b) Side view

Fig. 9 Grids of hull and cycloidal propeller

main thrust coefficient, torque coefficient, and lateral force coefficient in the wake and open-water conditions when e = 0.7, as shown in Fig.10. The figure shows that the hull wake has insignificant effects on the main thrust coefficient and torque coefficient of the cycloidal propeller, but it remarkably influences the lateral force; under the working condition where the eccentricity e = 0.7, the lateral force drops significantly when the influence of the hull wake is taken into account, which may be explained by the improvement in the lateral force thanks to the symmetrical optimized arrangement of the cycloidal propeller at the stern.

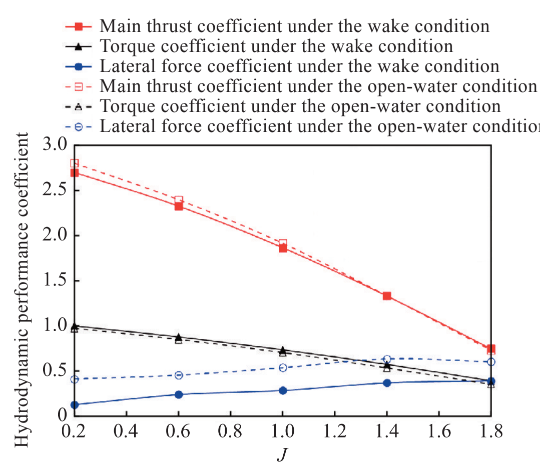

Fig. 10 Influence of hull wake on hydrodynamic performance of cycloidal propeller (e = 0.7)

4.3 Variation analysis of instantaneous loads of lateral force

Fig. 11 demonstrates the variation curves of the lateral force of the propeller and a single blade of a cycloidal propeller with the blade rotation angle in the wake field. It can be learned that the load changing trend under the wake condition is generally the same as that under the open-water condition, but the peak value of the single-blade lateral force decreases significantly under the influence of the hull wake, which contributes to the macroscopic decrease in the lateral force. Under the open-water condition, the lateral force fluctuates in one period, and the superposition of the multi-blade side thrust of the propeller can bring about the rolling of the hull; in the case of the ship-rear arrangement, the lateral force can be reduced by the installation of reverse-rotating propellers at a suitable position to offset the side thrust.

4.4 Analysis of ship-rear trailing vortex structure with cycloidal propeller

We analyze the variation characteristics of the trailing vortex of the ship-rear cycloidal propeller by use of different advance coefficients, namely, J = 0.2 (0.452 7 m/s), J = 1.0 (2.286 m/s), and J = 1.8 (4.114 8 m/s). Fig. 12 shows the trailing vortex structure of the ship-rear cycloidal propeller at different advance coefficients under the working con-

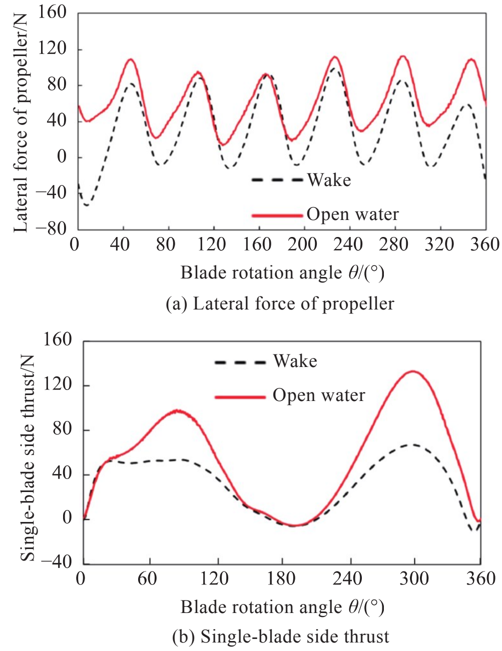

Fig. 11 Variation analysis of instantaneous load of cycloidal propeller and single blade (lateral force)

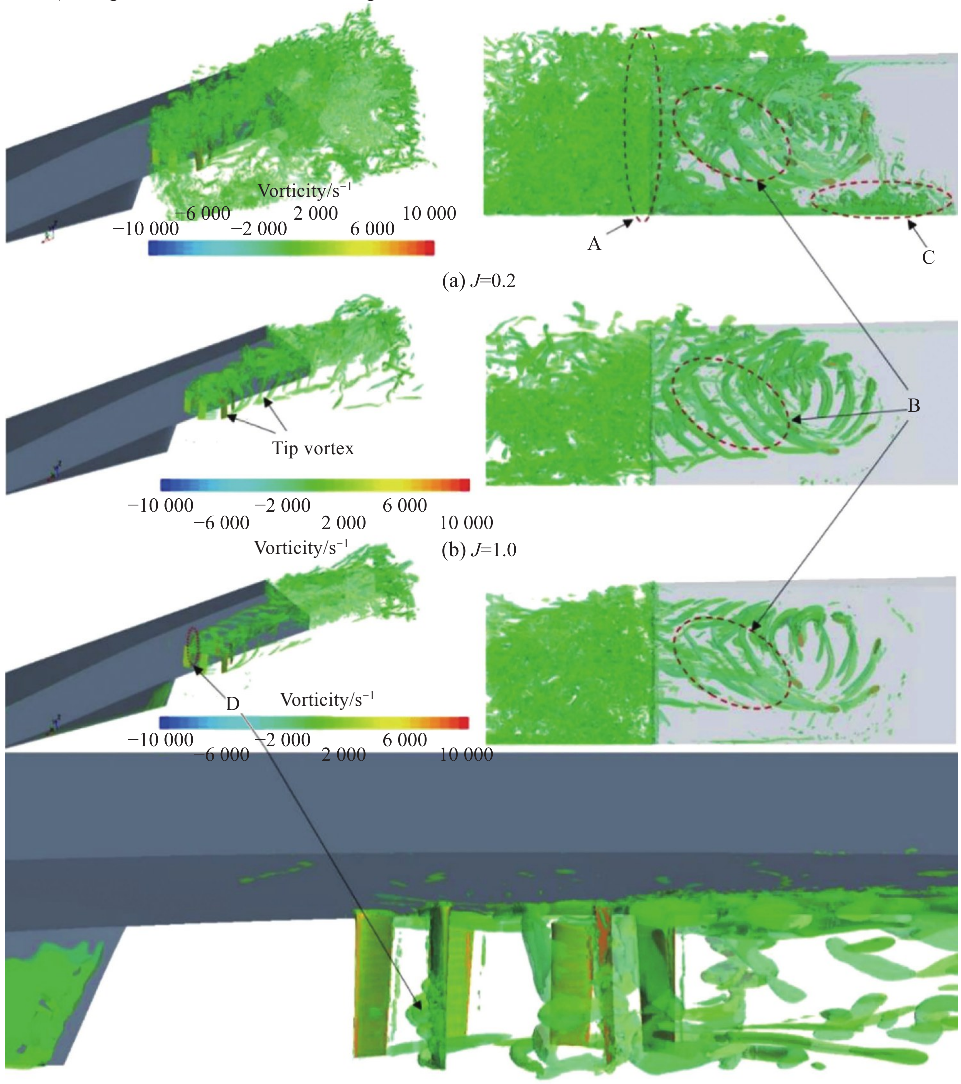

Fig. 12 Stern vortex structure of ship-rear cycloidal propeller at different advance coefficients (e = 0.7 and Q = 5 000)

dition where the eccentricity $e = 0.7$. The three-dimensional spatial structure of the vortex is displayed by the iso-surface of the Q criterion [11], where $Q = 5\ 000$. On the basis of the prediction method for ship-rear hydrodynamic loads of the cycloidal propeller, the calculation of the trailing vortex in this paper adopts a large eddy simulation, without considering the influence of the free surface.

It can be seen from Fig.12 that at a low advance coefficient ($J = 0.2$), due to the low inflow velocity, the trailing vortices separated from the blade airfoil tend to gather at the stern, and meanwhile, the vortices will also stick to the boundary of the plane of symmetry (Frame C). With the increase in the advance coefficient ($J = 1.0$), the tip vortices discharged from the blade root diffuse rapidly to the stern (Frame B). At a high advance coefficient ($J = 1.8$), the trailing vortices dissipate rapidly in the movement toward the stern. Moreover, the turbulent migration also accelerates with the increase in the advance coefficient, and the trailing vortices are inclined to shrink when drifting toward the ship. Due to the periodic circular motion of the cycloidal propeller's blades, the tip vortices falling off at the blade roots move to the stern in the form of a semi-circular strip and fuse with the vortices separated from the square stern (Frame A). As the inflow speed up, the angle between the tip vortex induced at the blade root and the symmetry plane of the midship keeps growing during diffusion. The figure also demonstrates that the flow separation on the surface of the blade airfoil can generate a wing vortex (Frame D) which, however, will dissipate rapidly after falling off.

5 Conclusion

This paper deduces the formulas for the multiple motion law of the blades by analyzing the operating principle of cycloidal propellers. Then it establishes the method for numerical simulation of the open-water hydrodynamic performance of cycloidal propeller by the sliding grid technique whose accuracy is verified in comparison with the test values. Finally, it studies accordingly the influence of the ship-rear wake field on the hydrodynamic performance of cycloidal propeller. According to the study, under the open-water condition, a rise in the eccentricity means a larger thrust coefficient and torque coefficient of cycloidal propeller, which is also accompanied by a wider range of the advance coefficient of the generated positive thrust. The variations of both propeller and single-blade instantaneous loads carry remarkable blade frequency characteristics, and at a certain eccentricity, the fluctuation amplitude of the main thrust and torque of the propeller increases with the decrease in the advance coefficient. The hull wake has insignificant effects on the main thrust and torque of cycloidal propeller, but it contributes to significant changes in the lateral force. The results of this study are of referential significance to the analysis of the blade strength of a cycloidal propeller and further studies on its hydrodynamic performance.

References

[1] BARTELS J E, JÜRGENS D I D. The voith schneider propeller: current applications and new developments [R]. Alexanderstr: Voith Turbo Marine GmbH & Company KG, 2006.

[2] JÜRGENS D, MOLTRECHT T. Cycloidal rudder and screw propeller for very manoeuvrable combatant [C]// International Symposium Warship 2001. London: RINA, 2001.

[3] CHEN X J. Research on the structure and performance optimization of cycloidal propeller [D]. Hangzhou: Zhejiang University, 2013 (in Chinese).

[4] HALDER A, WALTHER C, BENEDICT M. Hydrodynamic modeling and experimental validation of a cycloidal propeller [J]. Ocean Engineering, 2018, 154: 94−105.

[5] JÜRGENS D, HEINKE H J. Voith schneider propeller (VSP) -investigations of the cavitation behavior [C]// First International Symposium on Marine Propulsion. Trondheim, Norway, 2009.

[6] BROCKETT T. Hydrodynamic analysis of cycloidal propulsors [C]//Propellers/Shafting’91 Symposium. Virginia Beach, VA, USA, 1991.

[7] SHI K Y. Study of new cycloidal propeller based on stepper motor [D]. Hangzhou: Zhejiang University, 2011 (in Chinese).

[8] CD-ADAPCO. User guide STAR-CCM+version12.02 [M]. Melville, NY, USA: CD-ADAPCO, 2017.

[9] FICKEN N L, DICKERSON M C. Experimental performance and steering characteristics of Cycloidal Propellers [R]. USA, Washington D. C.: David Taylor Naval Ship Research and Development Center, 1969.

[10] PRABHU J J, NAGARAJAN V, SUNNY M R, et al. On the fluid structure interaction of a marine cycloidal propeller [J]. Applied Ocean Research, 2017, 64: 105−127.

[11] WANG Y Q, GUI N. A review of the third-generation vortex identification method and its applications [J]. Journal of Hydrodynamics (Ser. A), 2019, 34 (4): 413−429 (in Chinese).

船体伴流对直翼推进器水动力性能的影响

黄璐*, 陈奕宏, 曾柯, 刘竹青
中国船舶科学研究中心,江苏 无锡 214082

摘　要:[**目的**] 直翼推进器是一种特种推进器,其借助从船舶底部伸出并围绕垂直轴往复式摆动的桨叶产生精准且无级可调的推力,有必要研究敞水和伴流条件下直翼推进器的水动力性能。[**方法**] 首先,通过分析直翼推进器的工作原理,推导出叶片的多重运动规律公式;然后,基于RANS方程和湍流模型,采用滑移网格技术计算直翼推进器的敞水性能;最后,与试验值进行比较,验证直翼推进器水动力性能预报方法的准确性,并在考虑船体伴流影响的情况下,研究直翼推进器的非定常水动力性能。[**结果**] 由整桨瞬时载荷和单桨叶瞬时载荷变化规律的分析,显示叶片瞬时载荷存在明显的叶频特征,且随着进速系数的减小,桨叶主推力和转矩的波动幅值增大;船体伴流对直翼推进器主推力和转矩的影响较小,但侧向力变化显著。[**结论**] 研究结果对于分析直翼推进器的桨叶强度以及叶型优化具有借鉴意义。

关键词: 直翼推进器; 叶片多重运动; 船体伴流; 水动力性能